Semiconductor-to-metal transition in fluid selenium at high pressure and high temperature: An investigation using x-ray-absorption spectroscopy

Y. Soldo*
Laboratoire de Cristallographie-CNRS, av. des Martyrs 25, BP 166, 38042 Grenoble Cedex 09, France and Institut de Recherches sur la Catalyse, 2 av. A. Einstein, 69626 Villeurbanne, France

J. L. Hazemann
Laboratoire de Cristallographie-CNRS, av. des Martyrs 25, BP 166, 38042 Grenoble Cedex 09, France and LGIT CNRS, UJF, BP 53X, 38041 Grenoble, France

D. Aberdam
Laboratoire de Cristallographie-CNRS, av. des Martyrs 25, BP 166, 38042 Grenoble Cedex 09, France

M. Inui and K. Tamura
Faculty of Integrated Arts and Sciences, Hiroshima University, Higashihiroshima 739, Japan

D. Raoux
Laboratoire de Cristallographie-CNRS, av. des Martyrs 25, BP 166, 38042 Grenoble Cedex 09, France

E. Pernot
ESRF, Grenoble, France

J. F. Jal and J. Dupuy-Philon
Département de Physique des Matériaux, UCB Lyon I, France
(Received 25 July 1997)

In the vicinity of the critical point (1620 °C, 385 bars) the semiconducting properties of fluid selenium give way to a metallic state, as evidenced by conductivity and optical measurements. The need for accurate local information on the structure of fluid Se near its critical point moved us to perform x-ray-absorption measurements in its semiconducting and metallic phases in the pressure and temperature range up to 600 bars and 1550 °C. The good quality of the x-ray-absorption fine-structure (EXAFS) data, obtained thanks to the simultaneous use of a special cell developed for x-ray-absorption studies of liquids under those extreme conditions and of the high brightness of the focused x-ray beam available on the BM32 beam line at the ESRF, allowed us to use a nonharmonic analysis of the EXAFS data by using the cumulant expansion method, at least for the first coordination shell. Such an analysis gives reliable values of the coordination numbers, and moreover knowledge of the cumulant values up to sixth order permits us to reconstruct the shape of the first peak in the radial distribution function with a fairly good accuracy. Our EXAFS results clearly support the shortening of the Se chains approaching the metallic fluid phase at high temperatures. The reconstructed real distribution function $\rho(r)$, related to the twofold coordination along the chains, is quite asymmetric for $T \geqslant 800$ °C, with a tail extending down to the interatomic distance of Se dimers. In the metallic fluid state near the critical point, we find that the interatomic distance along the chains is strongly reduced in comparison to the semiconductor phase. This result is in agreement with the model suggested by Tamura *et al.* of a change from helical to planar chains at the phase transition. This planar geometry allows the lone pair orbitals to become π orbitals, which may overlap and form a strong covalent bond, resulting in a decrease of the interatomic distance. In addition, a main structural change in going from the semiconductor to the metallic fluid state is the appearance of a new bond at a significantly larger distance about 2.9 Å. It most probably implies the presence of a third neighbor for a large fraction up to 30–50 % of the Se atoms, which should be related to interchain interactions and form a network in the metallic phase. [S0163-1829(98)08401-X]

I. INTRODUCTION

While tellurium undergoes a semiconductor- (SC)- to-metal (M) transition upon melting, liquid selenium stays as a semiconductor up to high temperatures and high pressures. Figure 1 shows a pressure-temperature phase diagram of Se with contours of constant dc conductivity. In the Se liquid phase near its melting point, the twofold coordination in helical chains found in trigonal crystalline Se is largely preserved as evidenced by neutron- and x-ray-scattering data.[1–7] Thus, at moderate temperatures with respect to the critical point (1620 °C, 385 bars), Se is an example of a liquid semiconductor with purely covalent bonding. As temperature and pressure rise while staying below the critical region, the Se

 © 1998 The American Physical Society

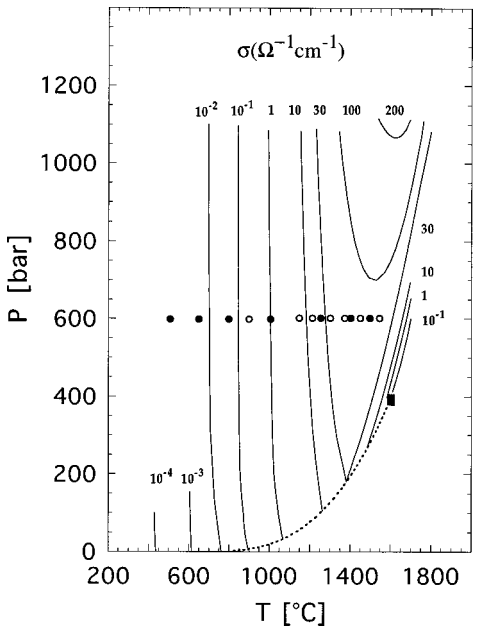

FIG. 1. Constant dc conductivity in liquid and supercritical fluid Se. The data are taken from Ref. 8. The solid square is the critical point, and the dashed line separates the liquid from the gas phase regions. Open and solid circles give the P and T values for the EXAFS measurements realized with and without a horizontally focused beam, respectively.

chains become shorter[8] and the dc conductivity becomes larger. When temperature and pressure are raised up to the vicinity of the critical point, the semiconducting properties give way to a metallic state, as evidenced by conductivity[9] and optical[10] measurements. The mechanism of this SC-M transition is still controversial, mainly because of the lack of a detailed structural knowledge in this P-T region, since x-ray or neutron diffraction as well as extended x-ray-absorption fine-structure (EXAFS) measurements are exceedingly difficult under these extreme conditions. It has been speculated that the metallic state in the high-temperature and high-pressure region is induced by the occurrence of threefold-coordinated centers which connect branched chains and which should be created in large number.[11] However, recently, Tamura and Hosokawa[5,6] succeeded in performing x-ray-diffraction measurements in the energy dispersive mode using an x-ray tube up to 1500 °C and 800 bars. The results showed that the Se coordination number for the first shell is slightly smaller than 2 in the metallic region, excluding the occurrence of a significant amount of threefold-coordinated centers with interatomic distances close to the regular intrachain interatomic distance at about 2.3 Å. Accordingly, they suggested a model of short twofold-coordinated chains with a planar zigzag conformation. In agreement with a previous theoretical study,[12] they argued that such a planar chain would result in a metallic state.

Although their x-ray diffraction experiments give very important information on the local structure of metallic fluid Se, the limited available range of the scattering vector (q) (until about 10 Å^{-1} at the highest temperatures) does not yield a satisfactory resolution in the determination of the coordination numbers and of the interatomic distances. So the need for accurate information on the local structure moved us to perform XAFS measurements in the semiconducting and metallic phases of fluid selenium, in order to make use of the high sensitivity of EXAFS to small changes in the local order due to the larger available range of the photoelectron momentum (k) ($q=2k=22$ Å^{-1}). EXAFS experiments have already been performed in the liquid semiconductor state[13] as well as in the vapor phase.[14] However, to our knowledge, no data are available in the metallic fluid one. We thus performed x-ray-absorption spectroscopy (XAS) measurements in the temperature and pressure range up to 600 bars and 1550 °C. Such measurements at high pressure and temperature, where the EXAFS modulations are extremely weak, are only possible because of the high brilliance of the x-ray source available at the European Synchrotron Radiation Facility (ESRF) at Grenoble, France.

II. EXPERIMENTAL CONDITIONS

The XAFS measurements have been performed in transmission mode using the spectrometer installed by the French Collaborative Research Group on the BM32 beam line at the ESRF. The storage ring was operated at 6 GeV in the multibunch mode with a 200-mA current. The beam line optics incorporates a Si(111) double-crystal monochromator, with an axis angular resolution of 1×10^{-4} rad. This resolution allows us to get an energy step of about 0.12 eV in the energy range of the experiment. The horizontal focusing of the beam fan is performed by sagitally and dynamically bending the second crystal of the monochromator,[15] while the vertical focusing is obtained thanks to a Ni-coated mirror installed upstream the monochromator, which is also used to reject the higher harmonics. The beam size at focus is about 300×300 μm.

The intensities I_0 and I of the incident and transmitted beams were monitored through the measurement of the intensities scattered by a kapton foil. Each measurement is performed using two Si diodes located above and below the x-ray beam to compensate for any slight motion of the focused beam during an energy scan.

We registered the XAFS spectrum for crystalline Se at room conditions as a standard, as well as that for liquid Se at 100 bars and 500 °C. Then a series of spectra was recorded in the fluid covalent and metallic states. In the fluid state, the SC-M transition occurs over a rather broad range of temperature and pressure as is shown by the rather continuous change in the conductivity (see Fig. 1). Actually, we define the SC-M transition parameters at the onset of the transition where the conductivity reaches about 30 Ω^{-1} cm^{-1}. Thus, as shown in Fig. 1, the XAFS measurements, which we made at 600 bars and at various temperatures ranging from 500 to 1550 °C, allow us to go through the SC-M transition. The measurements were performed on two different occasions, one by using a vertically and horizontally focused x-ray beam and the other with no focalization in the horizontal plane.

The experimental conditions of high pressure and high temperature were achieved using an internally heated high-pressure vessel made of super-high-tension steel, similar to the one described by Tamura *et al.*[16] The incident and transmitted x-ray beams go through 5-mm-thick Be windows. The

vessel is pressurized by He gas, which has a low absorption for x-ray photons in the energy range of the Se *K* edge. A high purity grade (99.9999%) of He gas is needed to minimize the risk of oxidation at high temperatures. The pressure is measured with absolute pressure transducers, having an accuracy of $\pm 0.3\%$ full scale, which can be used up to 700 bars. The high-purity-grade (99.999%) Se sample is contained in a cell made from polycrystalline sapphire,[16] which is connected to a reservoir and is located at the center of the high-pressure vessel. Its thickness, 30 μm, has been chosen so that the jump at the absorption edge is about unity. It is heated by a Mo wire. The temperature is measured at three locations by *B*-type thermocouples (Pt/Rh 30%, Pt/Rh 6%), which are in close contact with the sapphire walls enclosing the fluid sample. The temperature regulation is achieved using an Eurotherm 900 HP controller having an accuracy of $\pm 0.1\%$ full scale. The reservoir is heated by a wire of a Fe-Cr alloy and kept at 300 °C during the XAS recording. The sample gap was filled with flowing liquid selenium by pressurizing the reservoir following the procedure described in Ref. 16. We checked that the liquid sample completely filled up the sample gap by means of a fluorescent screen and an optical camera put downstream the high-pressure vessel, which gave an image of the sample thanks to its x-ray absorption.

III. XANES AND EXAFS RESULTS

Conductivity as well as optical measurements indicate that, at 600 bars, the SC-*M* transition starts to occur between 1000 and 1300 °C,[9,10] the conductivity being the highest around 1500 °C, as is shown in Fig. 1. In this temperature interval, the x-ray appearance near-edge structure (XANES) spectra exhibit significant changes as shown in Fig. 2(a). First, beyond about 10 eV above the edge rise, the amplitude of the XANES oscillations decreases with increasing temperature, suggesting a higher disorder at a medium-range scale. Second, the absorption edge undergoes a shift towards lower energies by about 0.6 eV, without a significant change in height and width of the white line. The strong correlation between the energy shift and dc conductivity of fluid Se as a function of *T* is shown in Fig. 2(b): The energy shift is a clear signature of the SC-*M* transition. As expected, this shift, which is related to the energy shift of the conduction band, is smaller than the optical gap in the semiconductor state, which is about 1.8 eV (Ref. 17) at 250 °C and 1 bar. The shift implies a decrease, and ultimately the disappearance, of the gap found in the semiconductor state. Thus we point out that it allows us to monitor directly the phase transition.

As is shown in Fig. 3, the EXAFS oscillations, as well as the XANES ones, are severely damped as the temperature increases because of the substantial increase of the Debye-Waller factor. However, even at the highest temperatures, they are still clearly displayed. This increase in the local disorder is evidenced by looking at the modulus of the Fourier transform (FT) of the EXAFS signal, which exhibits peaks related to the distribution of interatomic distances. From Fig. 4, it is already possible to get some qualitative information about the SC-*M* transition. At 600 bars, in the temperature range 500–1000 °C, all the FT's exhibit a single

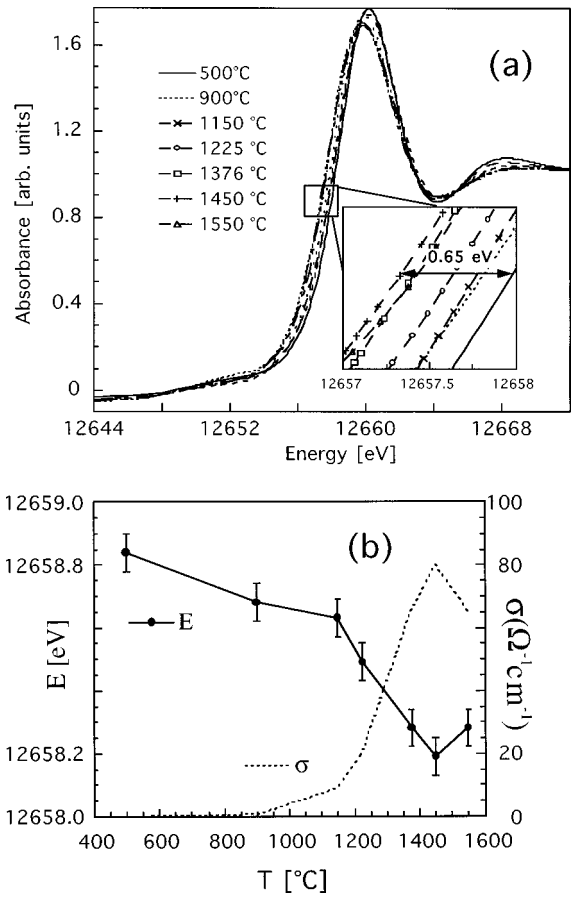

FIG. 2. Normalized XANES spectra (a) and edge energy *E* and dc conductivity σ (b) in the semiconductor range and in the metallic one. The values for the conductivity have been obtained from Fig. 1 by interpolation.

peak, the position of which does not significantly move. However around 1250 °C, in the same temperature interval where a shift in the absorption edge is observed, two significant changes occur in the FT signal. First, the peak position shifts towards a lower distance by about 0.05 Å. Second, a second shell clearly appears, as shown by the arrow in Fig. 4. Its position corresponds to an interatomic distance larger than the first one by about 0.6 Å. As temperature rises be-

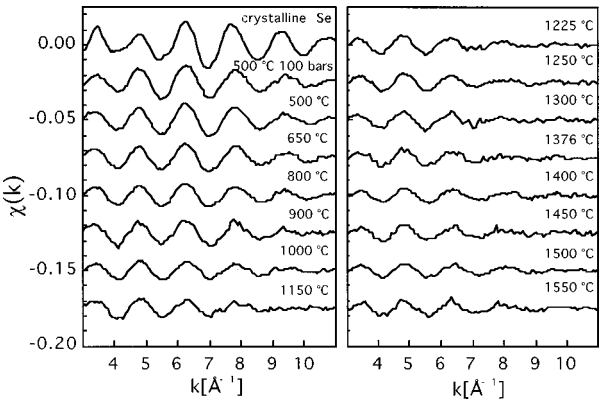

FIG. 3. EXAFS spectra. All measurements for fluid Se have been performed at 600 bars, except the first one at 500 °C and 100 bars. The crystalline Se spectrum has been recorded at normal conditions.

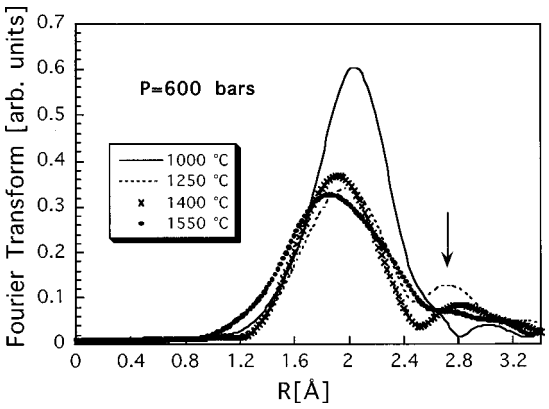

FIG. 4. Modulus of Fourier transforms of the EXAFS signals for liquid Se at 600 bars and various temperatures. A k^2 weighting factor and a Kaiser window ($\tau=2.5$) have been used to calculate the FT.

yond 1250 °C, its intensity strongly decreases, because of the increasing thermally induced local disorder.

Finally, we point out that the period of the XANES oscillations in the neighborhood of the absorption edge corresponds to the interatomic distance at about 2.3 Å, so that they are due to single-scattering processes and are just regular EXAFS modulations in the low-k range. The multiple-scattering processes seem to be destroyed by the high level of the thermally induced disorder, so that, unfortunately, the XANES features do not carry information on the medium-range ordering.

IV. DATA ANALYSIS USING THE HARMONIC APPROXIMATION

In the single-scattering approximation, the EXAFS amplitude $\chi(k)$ is given as a function of the electron wave number k (Å^{-1}) by the following expression (for simplicity, we refer to one shell of neighbors only):

$$\chi(k)=\frac{S_0^2}{k}\,N\,\mathrm{Im}\left\{F(k,\pi)e^{2i\delta(k)}\int_0^\infty \rho(r)\,\frac{e^{-2r/\lambda}}{r^2}\,e^{2ikr}dr\right\}, \tag{1}$$

where S_0^2 is the amplitude reduction factor introduced to account for many-body effects, $\delta(k)$ is the central atom phase shift, and $F(k,\pi)$ is the complex backscattering amplitude. Here $\rho(r)$ is the real radial distribution function (RDF) and N is the coordination number. With this notation, $\rho(r)$ is normalized in such a way that $\int\rho(r)dr=1$. The damping term $e^{-2R/\lambda}$ is due to inelastic losses in the scattering process, with λ being the inelastic mean free path of the photoelectrons.

Formula (1) shows that, actually, EXAFS does not sample the real RDF $\rho(r)$, but a so-called ''effective distribution'' $P(r,\lambda)$, where

$$P(r,\lambda)=\rho(r)\exp(-2r/\lambda)/r^2. \tag{2}$$

In the harmonic approximation, this distribution is expanded up to its second momentum C_2, usually noted as the square of the Debye-Waller parameter σ^2, so that one gets the usual formula

$$\chi(k)=S_0^2\,\frac{N}{kr^2}\,|F(k,\pi)|e^{-2k^2\sigma^2}e^{-2r/\lambda}\times\sin[2kr+2\delta(k)+\arg F(k,\pi)]. \tag{3}$$

So we first analyzed the EXAFS data within the harmonic approximation using the SEDEM package.[18] In that case, the disorder is taken into account by the Debye-Waller factor $\exp(-2k^2\sigma^2)$. First, the FT's of the EXAFS signals $k^2\chi(k)$, after weighting by k^2, have been performed using a Kaiser window with the τ parameter equal to 2.5 and using data between about $k=1.5$ and 12 Å^{-1}. Then, in order to filter the structural contributions of atom shells, the peak in the FT has been isolated and back transformed in k space.

The amplitude reduction factor S_0^2 is fixed to 1. To evaluate the electron inelastic mean free path $\lambda(k)=\gamma/k$, we made a polynomial fit of the reference spectrum (liquid Se at 500 °C and 100 bars) using the phases and backscattering amplitude from tabulated values of McKale *et al.*[19] We assumed the coordination number and the first neighbor interatomic distance equal to 2 and 2.33 Å,[6] respectively. The γ parameter is assumed to be constant whatever the temperature and pressure. This fit of the reference sample using the values of McKale *et al.* also yields an estimation of the Debye-Waller factor for the reference sample. We obtain $\sigma=0.096$ Å. Using these values, we have then extracted from the reference spectrum the total phase shift $2\delta(k)+\arg F(k,\pi)$ and the modulus of the backscattering amplitude $|F(k,\pi)|$.

We used a standard fitting procedure in order to determine the structural parameters such as the bond length r, coordination number N, and Debye-Waller parameter σ. For all spectra, the fits have been made over a k range from about 3 to 11 Å^{-1}. When two shells were present ($T\geqslant 1100$ °C), a two-shell fit has been performed.

We made an estimate of the noise in the $k^n\chi(k)$ data by computing the difference between the raw experimental EXAFS signal and the filtered one, which is supposed to contain the whole structural information. The statistical error is taken as the root-mean-square value of this difference.

The acceptability of the fit results has been tested from a statistical point of view using the χ^2 test and weighting the χ^2 values by the estimated statistical noise. To estimate the uncertainties on the parameters, we used the constant χ^2 boundary method,[20] which takes into account both the experimental statistical noise and the correlation between pairs of parameters. The elements of the covariant matrix, weighted by the statistical noise, allow one to draw the elliptic confidence region in the two-dimensional space associated with the pair of parameters considered. This ellipse defines the region where the probability distribution for the two parameters is larger than a certain value. For our estimation of the error bars, this value is set to 68%. The width and height of the smallest rectangle containing the ellipse are an estimation for the error bars of the two parameters. Of course, in order to have a valuable estimation of the uncertainty in a given parameter, it is necessary to consider its correlation ellipses with any other parameter to which it may be significantly correlated and then to select the largest uncertainty.

The results obtained for the first shell using the harmonic

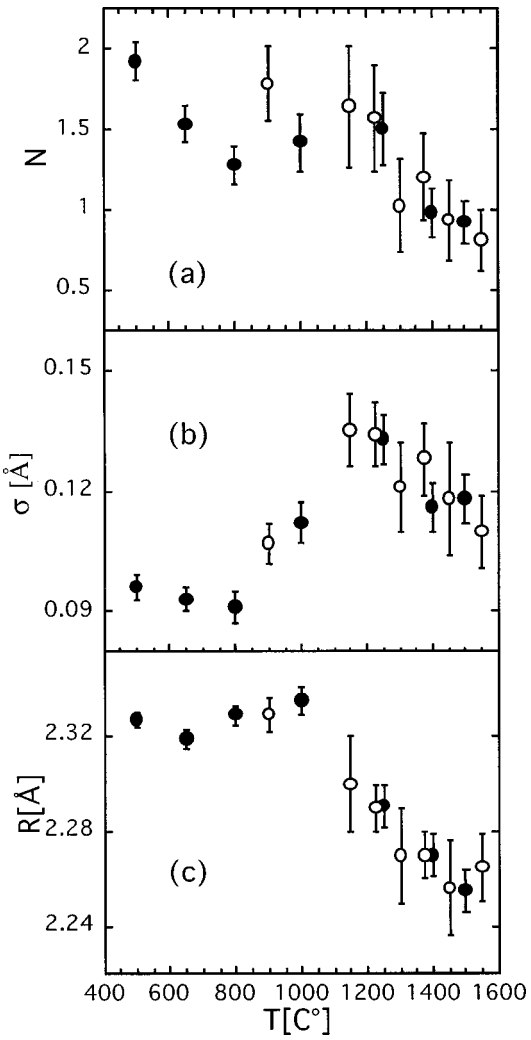

FIG. 5. First-shell coordination number (a), Debye Waller parameter (b), and interatomic distance (c) determined in the harmonic approximation. Solid and open circles refer to data obtained using a horizontally focused and unfocused x-ray beam, respectively.

approximation are shown in Fig. 5, where the two sets of measurements using an unfocused and a focused beam are displayed. The uncertainty is, of course, worse in the unfocused mode because of a larger noise in the data, but both series of results are in a rather good agreement. Table I gives the structural parameters determined from the experiments performed with the focused beam, which are less noisy. The coordination number decreases from 2 to about 1.5 when the temperature increases up to 650 °C. Within the uncertainty, it stays almost constant at temperatures between 650 and 1250 °C with a statistically weighted mean value of 1.5. This corresponds to an average length of chains of four Se atoms, which is not unrealistic, though rather short. The chain length n is evaluated from the coordination number N by assuming a twofold coordination for all Se atoms except for those at the ends of the chain which are onefold coordinated, so that $N=2-2/n$. However, as shown in Fig. 5 and Table I, the coordination number extracted using the harmonic approximation decreases below 1 at temperatures higher than 1250 °C. This temperature dependence evidences a structural transition occurring in the temperature range around 1200 °C. A similar conclusion can also be derived by looking at the interatomic distance which stays constant at about 2.33 Å up to 1000 °C and decreases drastically at higher temperatures down to about 2.25 Å at 1550 °C. The Debye-Waller parameter stays constant with a mean value of about 0.095 Å at temperatures below 900 °C and increases at higher temperatures, to reach a maximum value of 0.135 Å at about 1200 °C. Surprisingly, it slightly decreases at higher temperatures, while the electric conductivity continuously increases. We note that the maximum of the σ values appears in the temperature interval where the phase transition occurs.

However, though the simple harmonic approximation gives interesting qualitative results, it is not suitable for a quantitative evaluation of the parameters, because of the large degree of local disorder evidenced by the large values of σ and it yields unreliable measurements of the coordination numbers, of the Debye-Waller factors and, to a lesser extent, of the interatomic distances. Actually, we note that the first-shell coordination number is certainly underestimated in the metallic state since it is smaller than 1. This would correspond to isolated Se_2 dimers, and this is unrealistic since, in the fluid state, short Se chains exist which lead to a coordination number close to 2. Moreover, this small coordination number is also in disagreement with the values determined from the diffraction experiment results performed by Tamura and Hosokawa,[5,6] which suggest a coordination number around 1.7–1.8, thus slightly smaller than 2. The present discussion points out the need to go beyond the harmonic approximation to correctly analyze fluids at such high temperatures.

Table II gives the values of the parameters obtained for the second shell within the harmonic analysis which give a clear indication about the existence of this second shell. Due to the weak amplitude of the EXAFS oscillations, their uncertainties are rather large. Within the uncertainties, it seems that the coordination number can be considered constant, with a mean value of 0.45 ± 0.15 neighbors. However, these values are an underestimation of the actual ones since we use the harmonic approximation, which, as we discussed for the first-shell case, yields too low coordination numbers for similar σ values. The second-shell interatomic distance obtained within the harmonic approximation does not change neither with temperature and, within a rather large uncertainty, is about 2.86 ± 0.04 Å. The structural interpretation of this second shell will be discussed in Sec. VII.

V. BEYOND THE HARMONIC APPROXIMATION: A CUMULANT EXPANSION

When the effective distribution $P(r,\lambda)$ cannot be approximated by a Gaussian one, the difference between the real and effective RDF's cannot be neglected. The use of the standard formula in the harmonic approximation can lead to significant errors. This occurs either if the real distribution $\rho(r)$ is not Gaussian or if it is too broad to neglect the asymmetry induced on $P(r,\lambda)$ by the other terms in Eq. (2). In order to go beyond the harmonic approximation, it is necessary to expand the effective distribution $P(r,\lambda)$ given in Eq. (2) to higher momenta than the second-order one. To do that, we use the so-called cumulant method introduced by Bunker.[21] We expand the logarithm of the characteristic

TABLE I. Structural parameters obtained for the first shell in the harmonic approximation and using the cumulant expansion up to C_6. The interatomic distances R_m are the mean values of the real RDF $\rho(r)$, calculated with the cumulants; δ is the asymmetry of $\rho(r)$, N is the coordination number, R the interatomic distance, and σ is the Debye-Waller parameter. We could correctly estimate the error bars only in the harmonic approximation. We considered both the experimental statistical noise and the correlation between the extracted parameters.

	Harmonic approximation			Cumulant expansion			
T [°C]	N	$10^{-2}\ \sigma$ [Å]	R [Å]	N	$10^{-2}\ \sigma$ [Å]	R_m [Å]	δ
500	1.91±0.12	9.6±0.25	2.327±0.003		No anharmonic effects		
650	1.53±0.11	9.3±0.3	2.319±0.004	1.74	10.3	2.35	−0.048
800	1.28±0.12	9.1±0.4	2.328±0.004	1.91	13.1	2.35	−0.167
1000	1.42±0.18	11.2±0.5	2.335±0.006	1.67	13.1	2.32	−0.143
1250	1.50±0.23	13.3±0.6	2.292±0.009		Not calculated		
1400	0.99±0.15	11.6±0.6	2.270±0.009	1.79	18.1	2.22	−0.200
1500	0.92±0.13	11.8±0.6	2.255±0.009	1.58	17.8	2.23	−0.167

function $\psi(2k)$, which is the Fourier transform of the effective RDF, in a series of powers of the electron wave vector k^n by using the so-called cumulants C_n.[22] We then get

$$\ln[\psi(2k)] = \ln \int_0^\infty P(r,\lambda) e^{2ikr} dr = \sum_{n=0}^{\infty} \frac{(2ik)^n}{n!} C_n . \tag{4}$$

C_0 depends on the normalization of the distribution. The C_1 and C_2 terms correspond to the mean value of the effective interatomic distance and to its variance, respectively. Higher-order cumulants measure the deviation of the distribution from a Gaussian behavior. They are zero for Gaussian distributions. C_3 measures the asymmetry of the distribution. The meaning of higher-order terms is less intuitive.

It is of course possible to express the EXAFS amplitude and phase as functions of the cumulants by using Eq. (1), odd and even cumulants determining phase and amplitude, respectively:

$$\begin{aligned}\chi(k) = {} & \frac{S_0^2 N}{k} |f(k,\pi)| \\ & \times \exp\left(C_0 - 2k^2 C_2 + \frac{2}{3} k^4 C_4 - \frac{4}{45} k^6 C_6 + \cdots \right) \\ & \times \sin\left(2kC_1 - \frac{4}{3} k^3 C_3 + \frac{4}{15} k^5 C_5 + \cdots + 2\delta \right. \\ & \left. + \arg F(k,\pi) \right) . \end{aligned} \tag{5}$$

The values of cumulants C_n and coordination number N can be obtained by a polynomial fitting of the phase difference $\Phi^u - \Phi^r$ and of the logarithm of the ratio of amplitudes, $\ln(A^u/A^r)$, of the EXAFS modulations for the unknown (u) sample and the reference (r) one, by means of the following relationships:

$$\ln \frac{A^u}{A^r} = \ln \frac{N^u}{N^r} + (C_0^u - C_0^r) - 2k^2 (C_2^u - C_2^r) + \frac{2}{3} k^4 C_4^u - \frac{4}{45} k^6 C_6^u + \cdots , \tag{6}$$

$$\Phi^u - \Phi^r = 2k(C_1^u - C_1^r) - \frac{4}{3} k^3 C_3^u + \frac{8}{15} k^5 C_5^u + \cdots . \tag{7}$$

Formulas (6) and (7) are obtained by assuming that the RDF is Gaussian for the reference sample, so that the harmonic approximation can be used in that case $(C_{n\geq 3}^r = 0)$.

Once the cumulants C_n are known up to order n, we can obtain the effective RDF by back Fourier transforming the expansion of $\Psi(2k)$ up to the k^n term. Then, to extract the real RDF $\rho(r)$, we choose the mean value $\lambda = 11.7$ Å of the electron mean free path $\lambda(k) = \gamma/k$ averaged over the k range $3-11$ Å^{-1} we considered in the fitting procedure for the extraction of the cumulant values.

Table I gives the structural parameters for the first shell obtained from such an anharmonic reconstruction[18] using the cumulant expansion up to C_6 and compares them with the corresponding values obtained using the harmonic approximation. To allow us to perform a cumulant analysis, the EXAFS spectrum has to extend over a wide enough k range

TABLE II. Structural parameters obtained for the second shell in the harmonic approximation at 600 bars and different temperatures: near-neighbor number (N), interatomic distance (R), and Debye-Waller parameter (σ).

T [°C]	N	R [Å]	$10^{-2}\ \sigma$ [Å]
1150	0.45±0.50	2.81±0.03	12±4
1225	0.3±0.4	2.89±0.03	11±5
1250	0.4±0.2	2.92±0.01	11±2
1300	0.5±0.4	2.83±0.03	11±4
1376	0.5±0.4	2.86±0.02	12±3
1400	0.4±0.4	2.92±0.02	13±3
1450	0.15±0.20	2.81±0.03	12±3
1550	0.5±0.4	2.82±0.02	11±3

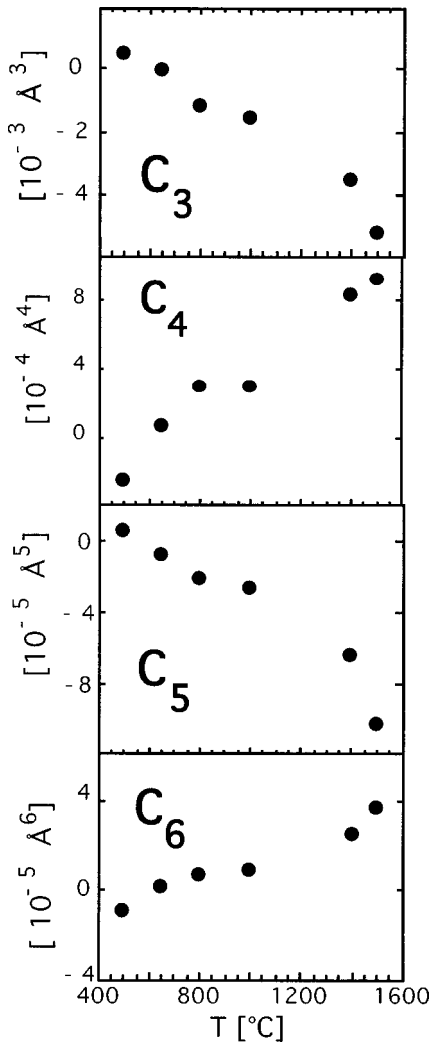

FIG. 6. Temperature dependence of the cumulants of the first coordination shell for $n \geqslant 3$.

with rather good statistics. This prevented us from analyzing the data obtained using an unfocused beam, so that all data in Table I refer only to spectra recorded using a focused beam. At 1400 and 1500 °C, the intensity of the second peak in the RDF is weak enough to allow us to accurately separate in R space the first shell from the second one. However, at 1250 °C, temperature at which the second peak is the most intense, it is not easy to do this and consequently we were not able to get reliable values of the cumulants, which do not depend on the filtering process in the R space. At $T \geqslant 1250$ °C, in the metallic state, we could analyze quantitatively only the first shell. The contribution of the second shell is too weak and too noisy to allow a cumulant expansion analysis.

Actually, at 500 °C and 600 bars, we found that the values of the cumulants are negligible for $n \geqslant 3$, so that there is no need to correct the results obtained with the harmonic analysis. At higher temperatures, we first calculated the cumulants only up to C_4, but in that case their behavior does not show a regular dependence with increasing temperature, which is not satisfactory.[23] For this reason, we then extracted the cumulants up to order 6. As Fig. 6 shows, they become larger as the temperature increases, which means that the distance distribution more and more deviates from a Gaussian one.

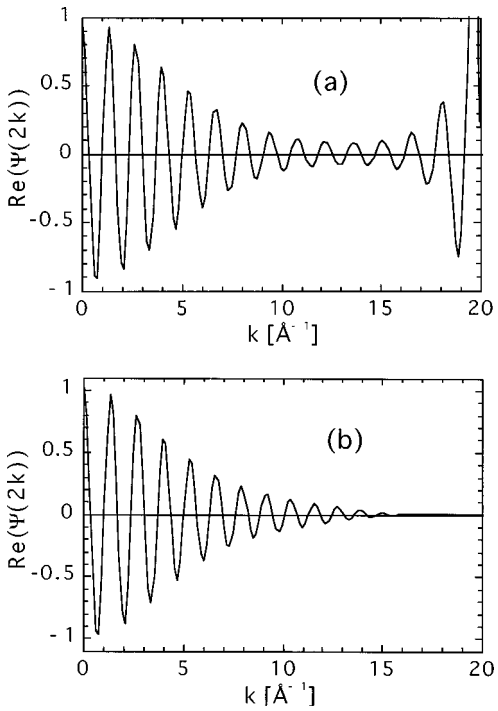

FIG. 7. Real part of the characteristic function $\Psi(2k)$ obtained for the experiment at 800 °C with the cumulants extracted up to C_4 (a) and up to C_6 (b).

We found that only for data at $T = 650$ °C are the results obtained by calculating the cumulants up to C_4 or up to C_6 almost the same. That is not the case at higher temperatures. In every case, we tested the convergence of the cumulant expansion up to C_6 using formula (4). As an example, Fig. 7 shows the real parts of the characteristic functions at 800 °C obtained using cumulants up to $n = 4$ [Fig. 7(a)] or $n = 6$ [Fig. 7(b)]: At large k values, there is no convergence to zero for the expansion calculated using the cumulants only up to C_4.

So, as shown in Table I and Fig. 8(a), using the anharmonic corrections until C_6 for data at $T \geqslant 650$ °C, we find that the coordination number N does not decrease drastically at the SC-to-M transition temperature despite this being suggested using the harmonic approximation. However, the local disorder strongly increases at the transition as is evidenced by the increase of the Debye-Waller parameter σ from 0.13 to 0.18 Å [see Fig. 8(b)].

We also reconstructed the real $\rho(r)$ distributions to get both their peak values $R_{\max}$ and the mean values of the interatomic distances R_{mean}, as well as the values δ of the asymmetry of the distributions. Here δ is defined as $\delta = (\omega_1 - \omega_2)/(\omega_1 + \omega_2)$, where ω_1 and ω_2 are the right and left half widths. As already suggested by the harmonic analysis, the interatomic distance is found to decrease by about 0.1 Å at the SC-M transition [see Fig. 9(a)]. However, already at 800 °C, in the temperature range below the transition, the mean interatomic distance R_{mean} is lower than the peak value $R_{\max}$ and a large negative asymmetry parameter δ is observed [Fig. 9(b)]. Figure 10 shows as an example the reconstructed $\rho(r)$ curves at 600 bars in the semiconducting state at 500 °C and in the metallic state at 1400 °C: The asymmetry at the highest temperature is evident.

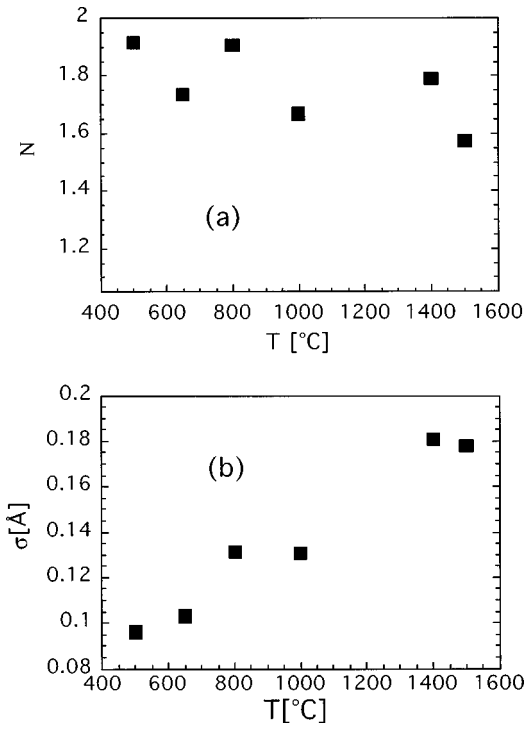

FIG. 8. Coordination numbers (a) and Debye-Waller parameters (b) obtained using the cumulant expansion for $T \geqslant 650$ °C and the harmonic analysis at 500 °C.

VI. DISCUSSION

The goal of this work is to try to characterize the local structure of the Se metallic fluid phase which is found in the vicinity of the critical point.

As far as the first coordination shell corresponding to an interatomic distance at about 2.3 Å is concerned, we have shown in this work that the anharmonic analysis gives reliable coordination numbers at all temperatures up to the highest one at about 1550 °C. Their values are found to be slightly lower than 2 already at rather moderate temperatures $T > 600$ °C. Despite the spread in their values, they seem to slowly decrease with temperature down to about 1.7 in the metallic phase. This is in good agreement with a previous x-ray-scattering experiment[5,6] performed in the same temperature range, but at a higher pressure of 1420 bars, which gave coordination numbers slightly smaller than 2 in the semiconductor state and around 1.7 in the metallic one. Our EXAFS results thus fully support a twofold intrachain coordination of the Se atoms at about 2.23 Å in the metallic phase and at about 2.35 Å in the semiconductor one.

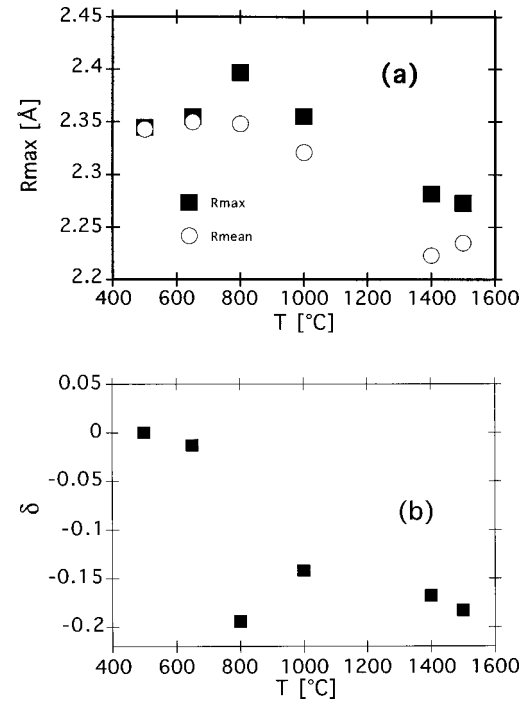

FIG. 9. Interatomic distances defined as the mean values (R_{mean}) and the peak values (R_{max}) of the reconstructed real distributions $\rho(r)$ of distances (a) and their asymmetry parameter δ (b).

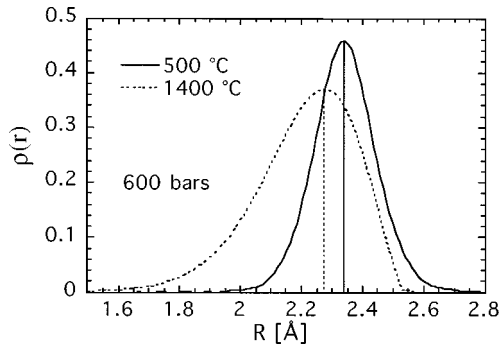

FIG. 10. Reconstructed real distribution functions calculated at 500 °C (solid line) and 1400 °C (dotted line), at 600 bars, using the cumulant expansion. $\rho(r)$ is clearly asymmetric at the highest temperatures.

The coordination number smaller than 2 may be related to finite lengths of the Se chains. The average chain length n can be calculated from the coordination number N by assuming that all the Se atoms along a chain are twofold coordinated except the two at the ends which are supposed to have a onefold coordination. One gets then $n = 2/(2-N)$. From this formula it is clear that as N approaches 2, even a small error bar ΔN on the coordination number yields a large uncertainty in the chain length. For this reason our EXAFS data cannot give an accurate estimation of the chain length, especially in the semiconducting state. Anyhow, the chain length seems to slowly decrease as the temperature increases, and in the metallic phase at 1500 °C, estimating ΔN on the basis of the uncertainties found within the harmonic analysis (see Table I), we find that $4 < n < 7$. We point out that this result is in a good agreement with previous NMR results[8] which estimate a chain length of seven atoms at 1550 °C and 400 bars.

As shown in Fig. 9(b), while the RDF's are symmetric below 700 °C, they become asymmetric at higher temperatures, with a tail extending towards small interatomic distances. In that case, the reconstruction of the actual RDF's evidences a distribution of the interatomic distances with a mean value R_{mean} about 0.05 Å smaller than the peak one at their maximum, as shown in Fig. 9(a). While the width of the RDF's increases from about 0.2 Å at 500 °C to about 0.4 Å at the highest temperatures around 1500 °C, the asymmetry ratio does not change much when increasing the temperature beyond 700 °C through the transition range around 1250 °C

and in the metallic state. This asymmetric distribution of interatomic distances suggests a distribution of the chain lengths with a significant proportion of shorter ones, since the interatomic distances are expected to decrease with the chain length to ultimately reach the value of 2.17 Å found by EXAFS for isolated Se_2 molecules in the vapor phase.[14] Actually, the reconstruction of the RDF's indicates that a noticeable fraction of the Se atoms forms very short chains, even in the semiconductor state, provided the temperature is higher than 700 °C. This is in agreement with simulations performed for that state by using a density-functional molecular dynamics method[11] or a tight-binding Monte Carlo simulation.[24] Both suggest, despite an average coordination number around 2, the presence of short chains in the structure of liquid semiconductor selenium.

The main structural changes associated with the electronic transition are, first, a significant decrease of the intrachain interatomic distance between nearest neighbors and, second, the occurrence of a second coordination shell at about 2.86 Å. We find that the nearest-neighbor interatomic distance decreases from about 2.35 ± 0.01 Å in the semiconductor state to 2.23 ± 0.01 Å in the metallic one. We point out that both the mean distance and the peak one decrease in the same way, as is shown in Fig. 9(a), so that their shortening cannot be attributed to an increase in the asymmetry of the RDF's towards lower distances. Therefore, our EXAFS results demonstrate without ambiguity a shortening of the interatomic distance in the metallic fluid state. This supports the hypothesis of a stronger intrachain bond in the metallic state than in the semiconductor one already suggested by Tamura and co-workers[6,7] on the basis of x-ray-scattering data at 1420 bars, indicating a similar, though smaller, shift from 2.33 to about 2.27 Å.

Our results also evidence the formation in the metallic state of a second coordination shell at 2.86 ± 0.04 Å. This distance occurs between the first (2.33 Å) and the second (3.44 Å) coordination shells in crystalline Se.[25] Thus its appearance in the metallic fluid state results from a structural change. We recall that its contribution to the EXAFS spectra is too weak to allow us to determine several cumulants with a reasonable accuracy. The harmonic analysis which we had to perform is certainly not quantitatively correct, especially as far as the coordination numbers are concerned. Therefore, our estimation of 0.45 ± 0.15 neighbors is an underestimation of the true coordination number. Nevertheless, it implies that a large amount of the Se atoms (30–50 %) are involved in such a bonding. This second shell might correspond either to a Se-Se interchain bond occurring at a larger distance than the intrachain one or to second neighbors along the Se chain. In that last case, we can calculate the bond angle along the chain from the interatomic distance 2.23 ± 0.01 Å and the second-neighbor one, 2.86 ± 0.04 Å. We get $80° \pm 1°$, which is not realistic for a p covalent bonding. Simple considerations show that the bond angle should be at least 90° in the case of pure p-wave functions and should actually be larger because of the hybridization of the $4p$ electrons with the $4s$ ones. Indeed, for helical chains in trigonal crystalline Se, its value is 103°. For planar zigzag chains, density functional calculations suggest a larger value of 124°.[12] Even considering the fact that within the harmonic analysis we probably make an error of the estimation of the second-neighbor distance, it should be of the same order of magnitude of the error we made for the first shell [0.05 Å in the worst case (see Table I), being the Debye-Waller factors of the two shells of the same order of magnitude]. But in order to have at least a bond angle of 90°, corresponding to a second-shell intrachain distance of 3.15 Å, we would underestimate it by about 0.3 Å. Thus, in our opinion, this coordination shell at 2.86 Å should be very likely associated with interchain and not with intrachain second neighbors. The interchain bonding would be related to the connection of two short Se chains through a threefold-coordinated Se atom. This bonding should be at least partly covalent to give a rather well-defined second coordination shell. We like also to point out that a large fraction of the Se atoms should be concerned with such a threefold coordination. Such a model would be in agreement with the *ab initio* molecular dynamics calculation of Kirchhoff *et al.*,[26] suggesting that for $T > 1370$ K there is a substantial penetration into the first coordination shell of interchain second neighbors, having an interatomic distance lower than 3.02 Å.

The resulting average local atomic structure would be a variant of the one proposed long ago by Cabane and Friedel[27] for liquid metallic tellurium. In agreement with the neutron-diffraction results by Tourand and Breuil,[28] they pointed out the importance of the interchain interaction and concluded that liquid Te has a network structure consisting of threefold-coordinated atoms at the high-temperature limit and at lower temperature, near the melting point, of a mixture of threefold and twofold bonding. However, it is to be noticed that there are several differences between the experimentally determined local structure of Se and Te. Recently, the structure of liquid Te was determined over a wide temperature range including the supercooled region by Menelle *et al.*[29] Their results suggest a splitting of the first coordination shell into two different kinds of atoms: the two covalently bonded atoms and a third atom at a slightly larger distance. It is now suggested that the two neighbors belonging to the same chain might be inequivalent: short and long bonds are observed by EXAFS (Ref. 13) and neutron-diffraction measurements.[30] A computer simulation by Bichara *et al.*[31] supports the observed local structure of liquid Te: a short-long alternation of the distances along the chain and a shortened interchain distance. They claim that, as the interchain distance is shortened, a resonance effect arises between the two lone pair orbitals on the two neighboring atoms bridging two chains which broadens their energy widths and fills the gap at the Fermi level, thus explaining the semiconductor-to-metal transition that is found for Te upon melting. Thus they conclude that the local structure of liquid Te is an asymmetric variant of the one proposed by Cabane and Friedel with three different neighbor distances.

This is not the case for fluid Se. In our work we do not observe any evidence for the presence of two different intrachain distances for Se, but an asymmetric distribution towards lower distances. Although the hypothesis proposed by Tamura and co-workers[6,7] explains the shortening of the first-shell interatomic distance, from the present stage we have to take into account interchain bonds in order to make clear the mechanism of the SC-M transition.

VII. CONCLUSION

This work demonstrates that it is possible to measure good-quality EXAFS spectra for liquids at very high temperatures despite the strong damping of their modulations with increasing the photoelectron energy. Actually, we succeeded in registering the weak EXAFS oscillations for fluid selenium up to $q=2k=22$ Å^{-1} in the vicinity of the critical point, up to 1550 °C at 600 bars. This large range in the scattering vector q yields a better resolution than the one obtained up to now by x-ray scattering and allows us to determine the shape of the first-neighbor atomic distribution. The good quality of the EXAFS data has been obtained thanks to the simultaneous use of a special cell developed for x-ray-absorption studies of liquids under those extreme conditions and of the high brightness of the focused x-ray beam available on the IF beam line at ESRF. Due to the efficient focusing optics, a 0.3×0.3 mm^2 beam spot is actually achieved at the sample location, allowing us to reduce the dimensions of the high-temperature and high-pressure vessel. This is a major advantage for safety reasons, as well as for ensuring a good homogeneity of the temperature over the illuminated part of the sample. We found that the quality of the EXAFS data obtained under these extreme conditions is good enough to allow us to perform a nonharmonic analysis of the EXAFS amplitudes by using the cumulant expansion method, at least for the first coordination shell. Such an analysis is mandatory because of the high level of local disorder. It gives reliable values of the coordination numbers, while the harmonic approximation yields drastically underestimated ones. Moreover, knowledge of the cumulant values up to sixth order allows us to reconstruct the shape of the first peak in the RDF with fairly good accuracy. This demonstrates the unique possibilities of EXAFS spectroscopy when performed on bright third-generation synchrotron sources to investigate the structure of liquids under extreme conditions and, especially, of liquid alloys.

Our EXAFS results clearly support the existence of short Se chains in the metallic fluid phase at high temperatures. They show that the first peak in the RDF, which is related to the twofold coordination along the chains, is quite asymmetric with a tail extending on the low-distance side up to the interatomic distance for Se dimers. This indicates a broad distribution of the chain lengths at high temperatures. Its width and shape, which are rather accurately determined using the cumulant method, yield a detailed information which theoretical simulations of fluid Se should reproduce.

In the metallic fluid state near the critical point, we find that the interatomic distance along the chains is strongly reduced in comparison to the semiconductor phase. This indicates a stronger bond in the metallic state, which might result in important changes in the electronic state. The most important changes concern the two lone pair electrons, which should give rise to a conduction band. By themselves, our results do not allow us to suggest a detailed possible mechanism. They are nevertheless in agreement with the model suggested by Tamura[6] of a change from helical to planar chains at the phase transition. This planar geometry allows the lone pair orbitals to become π orbitals, which may overlap and form a strong covalent bond, resulting in a decrease of the interatomic distance. They would give rise to a conduction process along the short chain. In addition, a main structural change in going from the semiconductor to the metallic fluid state is the appearance of a new bond at a significantly larger distance, about 2.9 Å. It most probably implies the presence of a third neighbor for a large fraction of the Se atoms, which should be related to interchain interactions and form a network in the metallic phase. The structure of metallic fluid Se would then resemble that of liquid tellurium with, however, two different interatomic distances corresponding, respectively, to intra- and interchain interactions. The metallic conductivity from chain to chain would then appear as a consequence of the resonance of the lone pair orbitals of two atoms belonging to neighboring chains. Such a model based on our EXAFS findings needs, of course, to be supported by other results and especially by x-ray-diffraction experiments performed up to large k values. Simulations of the structure and of the electronic properties of the metallic state in fluid Se would also be necessary.

ACKNOWLEDGMENTS

The authors are indebted to R. Argoud, R. Bruyere, and O. Geaymond for their helpful technical assistance.

*Electronic address: soldo@labs.polycnrs-gre.fr

[1] Y. Waseda, K. Yokoyama, and K. Suzuki, J. Phys.: Condens. Matter **18**, 293 (1974).
[2] G. Tourand, J. Phys. (Paris) **34**, 937 (1973).
[3] M. Edeling and W. Freyland, Ber. Bunsenges. Phys. Chem. **85**, 1049 (1981).
[4] R. Bellissent and G. Tourand, J. Non-Cryst. Solids **35&36**, 1221 (1980).
[5] K. Tamura and S. Hosokawa, Ber. Bunsenges. Phys. Chem. **96**, 681 (1992).
[6] K. Tamura, J. Non-Cryst. Solids **205–207**, 239 (1996).
[7] M. Inui, T. Noda, K. Tamura, and C. Li, J. Phys.: Condens. Matter **8**, 9347 (1996).
[8] W. W. Warren, Jr. and R. Dupree, Phys. Rev. B **22**, 2257 (1980).
[9] H. Hoshino, R. W. Schmutzler, and F. Hensel, Ber. Bunsenges. Phys. Chem. **80**, 27 (1976).
[10] H. P. Seyer, K. Tamura, H. Hoshino, H. Endo, and F. Hensel, Ber. Bunsenges. Phys. Chem. **90**, 587 (1986).
[11] D. Hohl and R. O. Jones, Phys. Rev. B **43**, 3856 (1990).
[12] M. Springborg and R. O. Jones, J. Chem. Phys. **88**, 2652 (1988).
[13] K. Tamura, M. Inui, M. Yao, H. Endo, S. Hosokawa, H. Hoshino, Y. Katayama, and K. Maruyama, J. Phys.: Condens. Matter **3**, 7495 (1991).
[14] S. Hosokawa, K. Tamura, M. Inui, M. Yao, H. Endo, and H. Hoshino, J. Chem. Phys. **97**, 786 (1992).
[15] J. L. Hazemann, K. Nayouf, and F. de Bergevin, Nucl. Instrum. Methods Phys. Res. B **97**, 547 (1995).
[16] K. Tamura, M. Inui, and S. Hosokawa, Rev. Sci. Instrum. **62**, 1382 (1995).
[17] S. Hosokawa, M. Yao, T. Yoshimura, and H. Endo, J. Phys. Soc. Jpn. **54**, 4717 (1985).
[18] SEDEM package, http://www.esrf.fr/computing/expg/subgroups/theory/xafs/aberdam.html
[19] A. G. McKale, G. S. Knapp, and S. K. Chan, J. Am. Chem. Soc. **110**, 3763 (1988).
[20] W. H. Press, B. P. Flannery, S. A. Teukolsky, and W. T. Vetter-

ling, *Numerical Recipes: The Art of Scientific Computing* (Cambridge University Press, Cambridge, England, 1986).
[21] G. Bunker, Nucl. Instrum. Methods Phys. Res. **207**, 437 (1983).
[22] G. Dalba, P. Fornasini, and F. Rocca, Phys. Rev. B **47**, 8502 (1993).
[23] G. Dalba and P. Fornasini, J. Synchrotron Radiat. **4**, 243 (1997).
[24] C. Bichara, A. Pellegatti, and J-P Gaspard, Phys. Rev. B **49**, 6581 (1994).
[25] R. W. G. Wyckoff, *Crystal Structures* (Interscience, New York, 1965), Vol. 1.
[26] F. Kirchhoff, M. J. Gillan, J. M. Holender, G. Kresse, and J. Hafner, J. Phys.: Condens. Matter **8**, 9353 (1996).
[27] B. Cabane and J. Friedel, J. Phys. (Paris) **32**, 73 (1971).
[28] G. Tourand and M. Breuil, C. R. Acad. Sci., Ser. II: Mec. Phys., Chim., Sci. Terre Univers **270**, 109 (1970).
[29] A. Menelle, R. Bellissent, and A. M. Flank, Physica B **156&157**, 174 (1989).
[30] T. Tsuzuki, M. Yao, and H. Endo, J. Phys. Soc. Jpn. **64**, 485 (1995).
[31] C. Bichara, J-Y. Raty, and J-P. Gaspard, Phys. Rev. B **53**, 206 (1996).